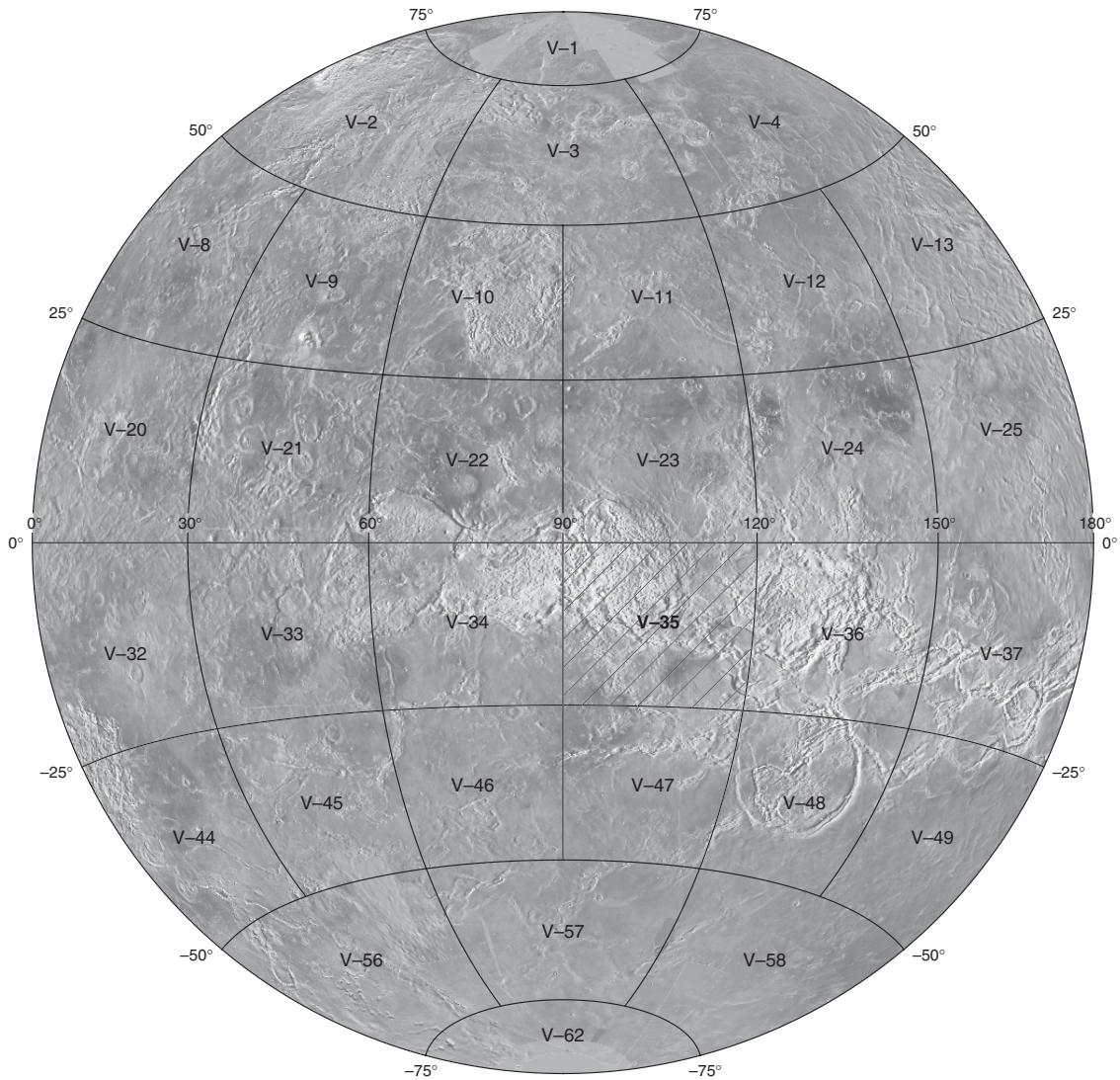


Prepared for the National Aeronautics and Space Administration

Geologic Map of the Ovda Regio Quadrangle (V-35), Venus

By Leslie F. Bleamaster, III, and Vicki L. Hansen

Pamphlet to accompany
Geologic Investigations Series I-2808



2005

U.S. Department of the Interior
U.S. Geological Survey

THE MAGELLAN MISSION

The Magellan spacecraft orbited Venus from August 10, 1990, until it plunged into the Venusian atmosphere on October 12, 1994. Magellan had the objectives of (1) improving knowledge of the geologic processes, surface properties, and geologic history of Venus by analysis of surface radar characteristics, topography, and morphology and (2) improving knowledge of the geophysics of Venus by analysis of Venusian gravity.

The Magellan spacecraft carried a 12.6-cm radar system to map the surface of Venus. The transmitter and receiver systems were used to collect three datasets: synthetic aperture radar (SAR) images of the surface, passive microwave thermal emission observations, and measurements of the backscattered power at small angles of incidence, which were processed to yield altimetric data. Radar imaging and altimetric and radiometric mapping of the Venusian surface were done in mission cycles 1, 2, and 3, from September 1990 until September 1992. Ninety-eight percent of the surface was mapped with radar resolution of approximately 120 m. The SAR observations were projected to a 75-m nominal horizontal resolution; these full-resolution data compose the image base used in geologic mapping. The primary polarization mode was horizontal-transmit, horizontal-receive (HH), but additional data for selected areas were collected for the vertical polarization sense. Incidence angles varied from about 20° to 45°.

High-resolution Doppler tracking of the spacecraft was done from September 1992 through October 1994 (mission cycles 4, 5, 6). High-resolution gravity observations from about 950 orbits were obtained between September 1992 and May 1993, while Magellan was in an elliptical orbit with a periapsis near 175 km and apoapsis near 8,000 km. Observations from an additional 1,500 orbits were obtained following orbit-circularization in mid-1993. These data exist as a 75° by 75° harmonic field.

MAGELLAN RADAR DATA

Radar backscatter power is determined by the morphology of the surface at a broad range of scales and by the intrinsic reflectivity, or dielectric constant, of the material. Topography at scales of several meters and larger can produce quasi-specular echoes, with the strength of the return greatest when the local surface is perpendicular to the incident beam. This type of scattering is most important at very small angles of incidence, because natural surfaces generally have few large tilted faces at high angles. The exception is in areas of steep slopes, such as ridges or rift zones, where favorably tilted terrain can produce very bright signatures in the radar image. For most other areas, diffuse echoes from roughness at scales

comparable to the radar wavelength are responsible for variations in the SAR return. In either case, the echo strength is also modulated by the reflectivity of the surface material. The density of the upper few wavelengths of the surface can have a significant effect. Low-density layers, such as crater ejecta or volcanic ash, can absorb the incident energy and produce a lower observed echo. On Venus, a rapid increase in reflectivity exists at a certain critical elevation, above which high-dielectric minerals or coatings are thermodynamically stable. This effect leads to very bright SAR echoes from virtually all areas above that critical elevation.

The measurements of passive thermal emission from Venus, though of much lower spatial resolution than the SAR data, are more sensitive to changes in the dielectric constant of the surface than to roughness. As such, they can be used to augment studies of the surface and to discriminate between roughness and reflectivity effects. Observations of the near-nadir backscatter power, collected using a separate smaller antenna on the spacecraft, were modeled using the Hagfors expression for echoes from gently undulating surfaces to yield estimates of planetary radius, Fresnel reflectivity, and root-mean-square (rms) slope. The topography data produced by this technique have horizontal footprint sizes of about 10 km near periapsis and a vertical resolution of approximately 100 m. The Fresnel reflectivity data provide a comparison to the emissivity maps, and rms slope parameter is an indicator of the surface tilts, which contribute to the quasi-specular scattering component.

OVDA REGIO QUADRANGLE

INTRODUCTION

The Onda Regio quadrangle (V-35), at lat 0° N. to 25° S. and long 90° to 120° E., encompasses approximately 8.4 M km² of complex geology with intricate volcano-tectonic relationships. The quadrangle was mapped at 1:5,000,000 scale under the Venus Geologic Mapping program. The northern part of V-35 includes south-central Aphrodite Terra, a high-standing, equatorial, plateau region that contains eastern Onda Regio and western Thetis Regio; the southern region, which is lower in topography, hosts Tahmina Planitia, Gauri Mons, Boszorkany Dorsa, the extensive flows of Inari Corona, and numerous other unnamed deformation centers and corona flows. The Kuanja, Ralk-umgu, and Vir-ava Chasmata system, a highly deformed east-trending zone, defines a geomorphic boundary between the high-standing crustal plateaus of the north and the southern low-lying plains (fig. 1, map sheet). Cross-cutting and embayment relations constrain the relative spatial and temporal relations of map units and tectonic structures within three geographic regions.

Within each region, individual tessera units, large corona flows, local volcano-tectonic complexes, chasmata deformation, and impact craters describe a coherent, or logically consistent, geologic history.

Detailed mapping was conducted using cycles 1, 2, and 3 Magellan synthetic aperture radar (SAR) images at C-MIDR and F-MIDR scale and Magellan altimetry, gravity, emissivity, and slope data where available and applicable (fig. 2, map sheet). FMAPs in both printed photographic and CD-ROM format provided the highest image resolution to view complicated volcanic and tectonic contacts. Stereo images, generated using cycle 1 and cycle 3 SAR stereo pairs (Plaut, 1993), and synthetic stereo images (fig. 3, map sheet), generated using topography and cycle 1 SAR (Kirk and others, 1992), proved useful in resolving the interactions of flows, primary and secondary structures, and topography. Incidence angles in V-35 provide a moderate range in viewing angle: cycle 1, 35.5°–45.2°; cycle 2, 24.9°–25.1°; cycle 3 stereo, 18.7°–24.5° (for more details see Ford and others, 1993).

MAPPING TECHNIQUES

Mapping began with the compilation of Magellan C-MIDR framelet scale images using Adobe Illustrator¹ 6.0 and 8.0 and progressed to the use of a synthetic stereo (Kirk and others, 1992) cycle 2 base map with FMAP framelet inlays. Use of NIH Image software, with a set of macros developed by Duncan Young at Southern Methodist University, Dallas, Tex., proved very useful for integrating multiple data sets and for allowing interactive adjustment of image stretch for detailed mapping, a technique that is particularly critical for mapping subtle material unit and structural facies boundaries. Throughout the mapping, material units were treated separately from tectonic (secondary) structures, and we delineated the spatial distribution of each (Hansen, 2000) in order to avoid assumption that tectonic structures form at the same time as the material unit (typically volcanic).

Problems inherent to mapping in the Ovda Regio quadrangle include (1) radar artifacts related to extreme topography (lay-over and foreshortening), (2) numerous highly deformed zones that mask material unit boundaries, and (3) an abundance of local depositional centers (paleotopographic and contemporary topographic lows) where flows from various sources appear to coalesce and create a unit that is an amalgam of separate materials. As a result, some of these features are grouped, although such grouping is not meant to imply the formation of a single coherent unit emplaced as a single event. We assume that Venus could host only the three basic rock types we

observe on Earth: igneous, metamorphic, and sedimentary. The absence of surface water and the paucity of eolian erosion on Venus (for example, Kaula, 1990) dismiss the idea that many surface rocks are of sedimentary origin. Furthermore, the apparent absence of widespread erosion suggests surface rocks are not likely exposed crustal metamorphic or intrusive igneous rocks. Thus, surface rocks most likely originated as extrusive igneous rocks, that is, volcanic flows. Exceptions to these flows include impact-related materials, eolian deposits, and atmospheric chemical precipitates; although these materials are present on Venus they are areally minor. Although one might argue that sedimentary or metamorphic rocks exist on the surface of Venus, we have come across no convincing evidence for widespread distribution of either of these two general rock types and we will consider them no further because no evidence supports their presence.

Venus geologic units (or “material units”; for example, volcanic flows, eolian deposits, crater deposits) are typically differentiated in Magellan data by patterns in SAR, emissivity, or rms slope data that reflect primary features such as lobate flows, mottling, or homogeneity. The first order task in mapping material units is to determine their spatial distribution and to examine contact relations between adjacent units (Wilhelms, 1990). Several problems must be kept in mind. Available data might inhibit unique distinction between different material units or may result in division of a single unit into two apparently different units (Hansen, 2000). For example, spatially separate lava flows may show similar radar, emissivity, or rms slope characteristics and, hence, one might conclude (incorrectly) that these units are time correlative. Alternatively, a single (or composite) volcanic flow unit emplaced within a single eruptive event may have both pahoehoe and aa flow facies and show radically different radar and rms slope signatures, and therefore they might be interpreted (incorrectly) as temporally distinct geologic units. Lumping versus splitting of material units depends in part on the understanding of process-dependent facies changes; fundamentally these potential problems are no different from those encountered in terrestrial mapping, although on Earth one may have more tools to address the problem. In an attempt to address these issues, we indicate flow direction data on the map; arrows indicate both the interpreted flow direction and location of flows, but also provide the user an indication of where we believe substantive evidence indicates the minimum limits of flow units. Users might treat such data in the same way that strike and dip information is treated on terrestrial maps—as a clear indication that the data were collected and interpreted at those specific locations. That is, the density and location of strike and dip symbology clearly indicate to a user not only the orientation of specific units, but also provide clear evidence of where a mapper has actually traversed the ground and where

¹Any use of trade, product, or firm names in this publication is for descriptive purposes only and does not imply endorsement by the U.S. Government.

map relations are projected from elsewhere. Dashed lines indicate the uncertainty of unit contacts. In many cases the exact location of a unit contact is important only in the context of a specific question; thus we encourage users of this map to examine such contacts in detail with specific individual questions in mind.

STRATIGRAPHY

Crustal plateau (high-standing, steep-sided, flat-topped, quasi-circular regions of thickened crust; Bind-schadler and others, 1992; Phillips and Hansen, 1994; Hansen and others, 1997) tessera terrains dominate the northern part of Ovda Regio quadrangle and represent the locally oldest deformed crust. Ovda Regio tessera terrain (unit **tO**), Thetis Regio tessera terrain (unit **tT**), and tessera terrain, undivided (unit **tu**) define local base materials (that is, a “stratigraphic” base), which are modified by subsequent volcanic and tectonic activities. The tessera units have been mapped as per the definition of tessera—as terrain containing two or more intersecting lineaments (for example, Barsukov and others, 1986; Basilevsky and others, 1986)—however, particular attention has been paid to the structural relationships preserved in these units. Structures within the tessera include one to two sets of ribbon structures (long, narrow, periodically spaced ridges and troughs; Hansen and Willis, 1996, 1998; Hansen and others, 2000) and broad folds or warps at various orientations dependent on both the specific tessera region and the geographic location within the tessera region (structural specifics to be given in a later section). Tessera is a tectonic terrain and is mapped based on a geomorphic description (much akin to gneissic terrains on Earth, which are differentiated because of the secondary process of metamorphism). The origin of the material unit(s) that hosts the ribbon-fold fabric is unknown but is presumably of volcanic origin as argued previously, although it was likely modified by thermal processes (Hansen and Willis, 1996, 1998). The tessera terrain map unit should not be viewed as a synchronously formed material unit but as an indeterminate (one or many) number of preexisting materials deformed into a coherent geomorphic feature. The tessera terrain of eastern Ovda Regio (unit **tO**) and in western Thetis Regio (unit **tT**) were divided based on their topographic signatures and on internal tectonic fabric patterns. Because subsequent tectonism and volcanism destroyed any embayment or cross-cutting relationships between the two provinces, temporal relations between Ovda Regio and Thetis Regio are unconstrained.

In addition to crustal plateau tessera terrain, tessera inliers (unit **ti**) have been mapped. The crustal plateau tessera terrains (units **tO**, **tT**, and **tu**) and the tessera inliers were differentiated based on (1) their size, (2) their relationship with the regional topography, and (3) their structural and spatial relationships. The crustal plateau

tessera terrains comprise three areally extensive masses that reside within broad topographic plateaus, whereas tessera inliers are locally high-standing (hundreds of meters) remnants, or kipukas, of tessera embayed by later volcanism. In some localities (for example, lat 15° S., long 99° E.), we assigned small tessera patches to Ovda Regio tessera terrain. These patches were included as part of unit **tO** on the basis of coherent structural fabric patterns and close spatial proximity to the majority of that unit. The unit **ti** label is reserved for tessera outcrops that lack structural fabric similarities to or topographic continuity with neighboring crustal plateau terrain.

Crustal plateau tessera terrains also are internally embayed by intratessera basin flow material (unit **fitb**; for example, Banks and Hansen, 2000); embayment patterns reveal detailed structural topography of ribbon-fold terrain. Intratessera basin flow material commonly preserves primary shield edifices and does not exhibit ribbons or folds, thus, at least the surface flows postdate ribbon and fold formation and therefore also postdate the material unit(s) that hosts the tessera deformation fabrics. Although spatially disparate intratessera basin flow material has been lumped into a single map unit, it is not meant to imply that all intratessera basins formed at the same time.

Intratessera basin flow material and crustal plateau tessera terrains are flooded by flows that do not have any clear internal crustal plateau sources and occur marginally around the crustal plateau tessera materials. These flows, mapped as marginal intratessera flow material (unit **fitm**), generally lack shield edifices and, in places (for example, lat 4.5° S., long 104.5° E.), host some structures that resemble ribbons and folds; however, unit **fitm** blankets the structures, thus tessera structures may have been reactivated to deform unit **fitm**, which suggests unit **fitm** dominantly postdated the formation of tessera fabrics. Timing between the formation of units **fitb** and **fitm** is difficult to determine, and the relative order of emplacement may vary from location to location. Unit **fitm** flows may be attributed to similar emplacement processes as unit **fitb** and simply show a different surface morphology due to flow thickness and depositional environment, or they may be unrelated. Because shield field formation has yet to be well understood on Venus (for example, Addington, 2001), speculation into the subtle differences between unit **fitb** and unit **fitm** is unwarranted.

Ovda Fluctus flow material, members a and b (units **fO_a** and **fO_b**, respectively) are marked by a strong radar reflectivity contrast. Both flows display lobate margins and appear thick (tens to hundreds of meters; Schenk and Moore, 1992), however, member a has high radar backscatter, whereas member b displays low radar return. Both flow members embay and occlude structures within the tessera terrain of Ovda Regio. The mega-scale structure resembles the lobate and large-scale pahoehoe-like surface characteristics of terrestrial flows and provides

strong evidence of a northwestern flow direction for member a. We agree with Campbell and others (1999) in their interpretation that member a is likely 50 m to a few hundred meters thick based on the bright radar reflections from the steep flow margins. We also suspect that the multiple bright radar reflections represent multiple flow pulses as noted by the flow fronts and directional arrows on the map. Member b, however, displays little or no surface structure, thus making thickness estimates and flow directions difficult to determine. It is not known whether members a and b are the same material or if they are distinctly different materials; Arvidson and others (1994) and Campbell and others (1999) attribute the shift in radar brightness to topographic effects. These workers propose that the dielectric constant of the surface changes at an elevation of 6,054 km, causing higher than normal radar reflectance and returns to plains like Fresnel reflectivity above ~6,056 km. Although the unit distinction is based solely on radar reflectivity—contrary to normal practice—in this instance we feel that differentiation is warranted and we encourage further investigations into this interesting contact.

Mantling material, members a and b (units mm_a and mm_b , respectively) are radar bright and dark, respectively, and display an apparent topographic dependence on radar reflectivity. These units differ from the Ovda Fluctus flow units because they show no primary emplacement features and few secondary deformation structures, thus they are likely the result of some exogenic or atmospheric process rather than endogenic volcanism. Although these deposits could be ash-fall deposits, their correlation with topography must be explained. In addition, Venusian ash deposits are difficult to justify given the high surface pressures and likely low volatile content of lava. More likely, these units represent atmospheric precipitation of material directly onto high-standing regions; the radar differences again are attributed to the Fresnel reflectivity variations at 6,054 and 6,056 km.

The Lo Shen Valles flow material (unit fLS) also originates in the Ovda Regio crustal plateau near the far-western margin of V-35. Numerous calderas, pit craters, pit chains, and sinuous canali mark the source region for these flows. Flows contained within the crustal plateau tessera terrain follow topographic slopes and embay tessera structures filling local lows. Other flows flow south and across the crustal plateau margin. Paleotopographic slope breaks can be inferred by distinct changes in the flow morphology (lat 17.5° S., long 90.5° E.). A transition from the monotonous, moderately dark gray tone to a moderately bright lobate flow could reflect a facies change due to emplacement velocity. A sharp slope break, from gradual to steep, could change the velocity of flow emplacement and possibly lead to a transition from slowly emplaced pahoehoe lava to rapidly emplaced aa lava. These different lava facies have distinctly different

surface roughnesses reflected in different radar characteristics. The various radar bright and dark facies have purposely not been delineated, because their patterns are consistent with broadly synchronous emplacement; however, the reader is encouraged to examine the SAR images for detailed flow patterns and data.

Unit fLS , which lies across the boundary between V-34 and V-35 at long 90° E., makes up much of the material in Tahmina Planitia. Although predominately outcropping in eastern V-34, a significant portion of V-35's southwestern corner is covered by unit fLS . Near the southern extent of the unit, away from the crustal plateau, moderately spaced (10–30 km) north-trending ridges deform the flows. The ridge appearance changes subtly across the Lo Shen Valles flow material and basal flow material, member 2 (unit fb_2) boundary from sharp and distinct within unit fb_2 to mottled and faint in unit fLS . This change is interpreted as representing initial burial (which is also supported by local topographically influenced flow margins) of unit fb_2 ridges, which results in an overall decrease in structural relief and thus a subdued radar contrast. Unit fLS ridges appear to be the result of reactivation of the buried ridges from the underlying basal flows, thus providing additional temporal relations between unit fLS and the older unit fb_2 . Unit fLS terminates over 1,200 km away from its source in an apparent combination of topographically influenced and magma-supply-limited boundaries. Finely serrated flow margins (lat 19° S., long 93° E.), indicative of very thin, low viscosity flows, provide evidence of topographic influence of preexisting structures within unit fb_2 .

Two units underlie unit fLS in the south including the aforementioned areally extensive basal flow material, member 2 (unit fb_2) and the less extensive basal flow material, member 1 (unit fb_1). Unit fb_2 dominates the southwest corner of V-35 and the northeast portion of Tahmina Planitia. North-northwest-trending closely (2–5 km) and moderately spaced ridges and fine-scale (1–2 km) northeast-striking fractures deform unit fb_2 . The short structural wavelengths and the intricate embayment boundaries with unit fb_1 suggest that unit fb_2 consists of relatively thin flows.

Unit fb_1 is preserved due to its local elevated position; that is, it is preserved as kipukas. It outcrops predominately in a set of northeast-trending ridges; however, the western portion of unit fb_1 contains numerous shield edifices. This unit, despite the morphological differences along its trend, is not divided because of a lack of temporal relations between the primary shields and the secondary ridges. Both the shields and the ridges experience subsequent deformation by northeast-striking fractures, and both are embayed by unit fb_2 . Therefore, within the scale of this map and the scope of this study, both the shields and ridges represent an older base (either made of one or many materials) that has been modified by later

volcanism and tectonism.

Two shield units (shield flow material, members a and b; unit fs_a and unit fs_b , respectively) also occur within the southwest corner of V-35. Each unit displays moderate backscatter and mottled texture, and each hosts abundant shield edifices (quasi-circular constructs with centralized pits). Unit contacts represent the greatest density of shields and may not include every shield in the vicinity because the shield field unit boundaries are diffuse. Both shield units lack secondary structures observed in the neighboring units fb_1 , fb_2 , and fLS (north-trending ridges and fine fractures), thus we inferred that these shield units overlie and are, therefore, younger than the units they grade into. Shields occur in almost every type of terrain on Venus (for example, Crumpler and others, 1997; Addington, 2001) and, although individual shields most likely form by effusive volcanism and edifice construction, shield fields may form by different processes—reaction to broad thermal upwelling, that is, corona; radioactive decay (Hansen and Bleamaster, 2002); or volatile inclusion (Hansen, 2003). The shields included within these units may or may not represent a coherent emplacement mechanism isolated to a relatively short period of geologic time. Temporal relations between units fs_a and fs_b are unconstrained, as they lack embayment or structural cross-cutting interactions. Although these units are locally some of the youngest material and may have been emplaced at similar times, they should not be lumped into a time-stratigraphic unit based simply on morphological similarities (for example, Basilevsky and Head, 1998) as illustrated by Addington (2001).

Tahmina Planitia flow material (unit fTh), a radar dark flow unit, embays unit fb_2 . From a southern source in V-47, unit fTh flows display an intricate pattern of embayment margins with the surrounding units. Unit fTh flows follow fine-scale topographic variations to the point of wrapping around individual wrinkle ridges (lat 22.5° S., long 95° E.). Unit fTh displays evidence of reactivation of the underlying north-trending ridge structures that deform unit fb_2 . Unit fTh is also cut by northeast-striking fine fractures similar to those that cut unit fb_2 ; however, the fracture spacing is smaller. Given that fracture spacing could reflect layer thickness (Ladeira and Price, 1981), the fine-scale fractures suggest that the flows are potentially extremely thin; the fine detail of flow margins with topography is also consistent with thin flows.

Gauri Mons, a moderately sized (~ 150 km diameter) volcano marked by radiating fractures and flows (unit fG), is near the south-central portion of V-35. Unit fG embays and is bounded by deformed Boszorkany Dorsa basal material (unit bB) to the east and by chasmata/coronae flow material, undivided (unit $fchu$) to the north, south, and west. In addition to the radial fractures directly related to the emplacement of Gauri Mons, north-northwest-trending moderately spaced ridges and northeast-

striking fine fractures deform unit fG . Individual shields are designated on the map as small pluses; these mark a few isolated areas within unit fG that contain significant shield populations. These areas are not differentiated from unit fG because temporal relations indicate shield edifice formation before and after radial flows and structures from Gauri. Thus, shield emplacement in this area is related to Gauri Mons, and shield morphological differences result from variations in emplacement mode and local environmental effects.

Unit bB , as with unit fb_1 , has an elevated position above the surrounding flow material. The flows of unit bB are preserved in a set of north-northwest-trending ridges. As unit bB is preserved as kipukas, it is not known whether the surface material contained in this unit represents a single material unit emplaced as an isolated event or whether it is an amalgam of materials deformed into a coherent ridge belt. In either case, the important observation is that emplacement and deformation of unit bB into north-northwest-trending ridges predates the emplacement of Gauri Mons flow material, Inari Corona flow materials, members 1a, 1b, and 2 and the Jhirad impact.

Inari Corona flow materials, members 1a, 1b, and 2 (units fl_{1a} , fl_{1b} , and fl_2 , respectively) dominate the southeast corner of V-35. Inari Corona (lat 18° S., long 120.3° E.), a small (~ 200 km diameter) corona, is part of a much larger volcano-tectonic center that lies along trend of a corona and chasma chain that extends to the southeast toward Artemis Chasma in V-48. Although not all Inari flows can be traced back to Inari Corona, the flows are a combination of volcanic activity from the corona and the neighboring chasmata, which together display an intimate history of broadly contemporaneous volcanism and tectonism. Large radial sheet flows dominate the early stages of Inari activity (units fl_{1a} and fl_{1b}). A marked radar brightness contrast exists between most of the material assigned to units fl_{1a} and fl_{1b} , although the boundary is gradational especially in enhanced images. This boundary was constrained primarily on radar brightness, and in places it could be argued that the boundary does not exist. However, because unit fl_{1a} is considerably darker in single stretched SAR images, as with the base map, it was necessary to employ a myriad of individually stretched, high-resolution FMAP framelets. Varying the image processing stretch of this same area reveals considerable detail within each unit member. Unit fl_{1a} is deformed by many east-trending structures and hosts numerous channels that branch to the north. Following the channels to the south, they cross the unit fl_{1a} - fl_{1b} contact. This relation, in part, leads to the age ambiguity between units fl_{1a} and fl_{1b} . In order to make an age determination, one must first assume a mechanism for channel formation. Given that the channels are present in both units and cross the contact, the channels could be interpreted as postdating both flows (that is, by mechanical and thermal erosion

of extrusive lava). However, the channels could also represent an intricate plumbing system responsible for the distribution of the far-reaching Inari flows, thus resulting in a syneruptive relationship. Alternatively, the channels could represent remnant channels that were covered by younger lava and exposed by subsequent roof collapse. In fact, the channels in this region show a variety of temporal relations with the flows of Inari Corona, suggesting a long-lived process responsible for their formation, like that documented by Stewart and Head (2000) for Baltis Vallis. The intricate distributary patterns (at the unit fl_{1a} and unit fl_{1b} contact) and truncations (lat 22.5° S., long 114.5° E.) also argue for a diachronous history and advise caution in making temporal interpretations.

Inari Corona flow material, member 2 (unit fl₂) is dominated by channel- and fracture-fed flows that have digitate boundaries. These flows display a higher degree of radar contrast than the older Inari flows, which may either represent different individual flow fronts or facies changes due to variable emplacement.

Rosmerta Corona flow material (unit fR) dominates the northeast corner of V-35. Although Rosmerta Corona (lat 0° N., long 124.5° E.) is within V-24 quadrangle, emanating flows are responsible for much of the flooding in Thetis Regio. Topographic depressions in Thetis serve as local depositional centers for flows. In the north, where the Thetis Regio margin slopes to the north, Rosmerta flows embay and subdue tessera structures; in addition, flows from Rosmerta embay tessera terrain, undivided (unit tu). The Rosmerta flows show a wide variety of deformational patterns, ranging from undeformed (lat 3° S., long 118° E.) to areas having a mixture of intersecting extensional and contractional structures. Structural trends mirror those of the surrounding terrain, thus suggesting local structural reactivation. Flow arrows mark the extent of flows that can be directly traced to Rosmerta Corona; however, the unit fR contact has been drawn 700 km to the west of the flow arrows. This area is an example where multiple flows from multiple sources coalesced into a single depositional center. In this case, synthetic stereo images provided clues as to the source area for these distal flows. With the exception of late subsidence (postdating unit fR) centered at lat 3° S., long 118° E., Rosmerta flows follow a gentle topographic slope from the summit of Rosmerta Corona to the west. Apparently, following the local paleoslope, lava then flowed northward (lat 3° S., long 113° E.) and embayed unit tu. Near the west margin of unit fR, Rosmerta flows and small shields display various temporal relations (some shields predate, whereas others postdate the Rosmerta flows).

The western section of Turan Planum (lat 12.5° S., long 115° E.) hosts some of the smoothest material in V-35. Turan Planum flow material (unit fTr) comprises isolated radar dark flows that sit high within a structurally isolated basin, where they embay remnants of tessera ter-

rain, which was once part of Thetis Regio proper. Subsequently, isolated through-going, east-trending troughs cut the flows. Assuming that the Turan flows were emplaced smooth and featureless, which is consistent with observations at the best resolution, it is necessary to explain how the flows preserved their smoothness. One interpretation would conclude that because the flows are smooth and lack significant deformation, they are young. However, an alternative interpretation is that the flows are old and have simply not experienced the penetrative deformation displayed by the material to the north and south of Turan Planum. Stratigraphically, the flows overlie Thetis Regio, which represents thickened crust; structurally, the flows are surrounded by steep margins interpreted to be normal fault scarps. This combination of strength and isolation may lead to a partitioning of strain around the basin, much like ductile fabrics wrap around strong porphyroclasts in terrestrial metamorphic rocks.

Chasmata flow material, member a (unit fch_a; lat 14° S., long 118° E.), within eastern Turan Planum, similarly lacks the penetrative secondary structures associated with Vir-ava and Jana Chasmata. The absence of such structures, as discussed above, may be the result of young lava covering the majority of earlier formed structure or may be due to crustal heterogeneities. Chasmata flow material, member b (unit fch_b) superposes unit fch_a in this area and is therefore younger; however, their temporal relations only hold for this specific locality. Isolated occurrences of unit fch_b flows that emanate from fissures and cover preexisting chasmata structure are distributed throughout the chasmata. These flows are differentiated from their surroundings based on flow fronts and a lack of closely spaced fractures. The lumping of these isolated occurrences does not imply synchronicity.

Chasmata flow material, undivided (unit fchu) is an areally extensive unit that displays a variety of radar characteristics, embayment relationships, structural facies transitions, and temporal relations. Unit fchu contains flows from various sources; flow fronts may have never developed or were subsequently deformed, thus erasing evidence of the primary relationships between individual flows. Given that much of V-35 has experienced significant deformation, much of the area has ambiguous temporal relations and is included in unit fchu.

IMPACT CRATERS

Within V-35 quadrangle, nineteen impact craters range from ~2.0–50.2 km in diameter (table 1). Crater material, undivided (unit c) includes pristine crater floor material (radar bright), ballistic ejecta blankets, and impact structures (that is, walls, rims, central peak, and so on). Flooding of the crater interior, whether by impact melt or subsequent volcanic interactions, is mapped as flooded crater material (unit cf).

Most impact craters within the V-35 quadrangle have unconstrained timing relations; each crater is simply younger than the unit it impacts; however, in a few cases craters show temporal relations with surrounding volcanic or tectonic activity. Six craters occur within Ovda Regio tessera terrain and two others within Thetis Regio tessera terrain. None of these eight craters are deformed by the small-scale, short-wavelength, structural features (ribbons or folds); however, two craters—Jennifer (lat 4.6° S., long 99.8° E.) and Makola (lat 3.8° S., long 106.7° E.)—lie on the limbs of the broad-scale, long-wavelength marginal folds. These craters may have either impacted on the sides of the fold limbs or they may have been tilted during deformation. In either case, no evidence exists for an impact event occurring early during crustal plateau formation, which supports findings of previous studies (Gilmore and others, 1997; Ghent and Hansen, 1999; Hansen and others, 2000).

Other craters that show relative temporal relations with subsequent deformation or modification include the following: Teura and Denise (unit fLS), Jhirad (unit fl_{1a}), Maltby (unit fl_{1b}), Yonge and Gail (unit fchu), and an unnamed crater (lat 7.8° S., long 97.9° E.; unit tO). Each of these craters, except the unnamed crater, were modified by post-impact deformation. This places some constraint on the timing of the impact events that formed each crater. The impact event must be younger than the material they affect, yet older than the structural suite that deforms the crater. The unnamed crater is not deformed but displays relative timing indicators with unit mm_a. Because unit mm_a is topographically delimited (only precipitating on elevated regions), unit mm_a blankets the southern, elevated rim of the unnamed crater, whereas the floor is unmodified. This relationship places the impact event after tessera formation but before final deposition or precipitation of the mantling material, because deposition or precipitation could have been a time transgressive process. The impact could have occurred after deposition or precipitation began; however, deposition or precipitation must have continued after the impact event.

STRUCTURE

The V-35 quadrangle can be divided into three dominant structural suites—tessera or crustal plateau structures, chasma structures, and corona structures—and numerous local deformation patterns. Although individual structures within the greater part of each suite are typically distinct and differentiable, near their boundaries structural trends and morphologies commonly converge into one fabric, which suggests that late-stage deformation preferentially utilizes weaknesses in the crust imparted by the earlier structures. For this reason, caution must be taken when applying cross-cutting relations of structural trends to constrain temporal relations, because assump-

tions regarding the mechanism of formation may lead to false temporal interpretations.

Tesserae and Crustal Plateaus

Eastern Ovda Regio and western Thetis Regio are small parts of two much larger crustal plateaus. The surfaces of these crustal plateaus manifest as an intricate pattern of intersecting lineaments recognized as ribbons, folds, and graben. Within the tessera terrains, shear fracture ribbon (Hansen and Willis, 1998) wavelength, marked by ribbon ridge width (<2.5 km), suggests a shallow depth to the brittle-ductile transition (BDT) at the time of ribbon formation (Hansen and Willis, 1998), whereas the greater fold wavelength might imply a depth to the BDT of ~6 km (Brown and Grimm, 1997). Given the spatial association of ribbons and folds, ribbon structures likely predate fold formation (Hansen and Willis, 1998; Ghent and Hansen, 1999; Hansen and others, 1999).

Within portions of the Ovda tessera terrain (lat 7° S., long 101° E.), two nearly orthogonal ribbon suites trend northwest and southwest. Similarities in the ridge spacing of each suite reflect a similar layer thickness, indicating that the two ribbon suites likely formed broadly synchronously. Also contained in Ovda is an arcuate marginal fold belt that sweeps from the north near lat 0° N., long 103° E. to the southwest. These folds are parallel to sub-parallel, long (hundreds of kilometers), and moderately spaced (10–30 km). Interior to the marginal fold belt of Ovda (west of the plateau margin), the folds display much greater variety in orientation, length, and spacing. These two regions are domains II and III, respectively, of Ghent and Hansen (1999). Temporal relations between the fold suites and the ribbon suites are constrained again based on mechanical arguments. Within the arcuate marginal fold belt of eastern Ovda Regio, a near continuum of ridge wavelengths ranges from 2 to 30 km. This suggests that the earliest formed folds (shortest wavelength) were most likely formed contemporaneously with the ribbons and that, as deformation continued and the BDT moved downward, fold wavelength increased.

Although western Thetis Regio does not display a coherent set of ribbon fold relations within the V-35 quadrangle, the crustal plateau does display similar features. Ribbons generally trend due north throughout the crustal plateau, whereas folds within V-35 trend northwest (lat 9° S., long 112° E.) and north (lat 6° S., long 119° E.). Near the east boundary of V-35, folds merge into a single northwest trend and continue in this pattern to the east. Near the southern reaches of Thetis proper lies Jana Chasma, a 50-km-wide topographic low characterized by closely spaced fractures, pit chains, and volcanic flows, the result of corona and chasma development. Extensional strain, in the form of east-striking, south-dipping normal faults, related to the formation of Jana Chasma (a

branch of the much larger Kuanja, Ralk-umgu, and Vir-ava Chasmata system) served to separate a part of Thetis from the main crustal plateau. Within Turan Planum (lat 13° S., long 116.5° E.), tessera terrain remnants, once part of Thetis, crop out. The relatively low strain preserved within Turan Planum may be attributed to strain partitioning or to subsequent burial by later-stage volcanism.

Plateau tessera terrain, undivided (unit *tu*) lies between Ovda Regio and Thetis Regio. Distinction of this unit is based on its lower topographic relief and absence of structural fabric continuity with either Ovda or Thetis tessera terrains. Structural fabrics within this unit continue to the north in V-23 within a large plateau tessera block.

Chasmata

Kuanja, Ralk-umgu, and Vir-ava Chasmata, collectively, define an elongate (2,500 km long, 400 km wide) topographic low centered approximately at lat 15° S., long 110° E. and are characterized by a dense swarm of broadly undulating, locally anastomosing lineaments that trend nearly due east. Approximately 4 km of relief separate the flanks of the chasmata (~1–2 km above mean planetary radius) and the trough floor. The structural suite of the chasmata system includes pit chains, scalloped troughs, normal faults, and fractures. The presence of these structures and their spatial association with volcanic features (units *fchu*, *fch_a*, and *fch_b*; coronae and small volcanic edifices) suggest that the chasmata are a “coherent intrusive complex” (Walker, 1992) consisting of a rich history of contemporaneous volcanism and tectonism. Along the Kuanja, Ralk-umgu, and Vir-ava Chasmata system, structural development decreases to the west, which suggests that the rift has progressively deformed the area from the east to the west, or has unzipped to the west. Branching of the rift into two arms, one continuing to the west and the second veering north, near the southeastern Ovda Regio boundary also supports a westward migration. We interpret this bifurcation of the chasmata as the result of strain partitioning occurring when the chasmata encountered the thicker crust at the Ovda margin. Although the two arms may have developed independent of each other, heterogeneities in the lower crust between eastern Ovda and western Thetis likely provided a zone for deformation to follow.

Coronae

Corona magmatism and deformation play an important role in the geologic and resurfacing history of the V-35 quadrangle. Inari Corona, in southeastern V-35, is responsible for large-scale deformation and large outpourings of lava. Inari Corona illustrates the detailed relationships between tectonism and volcanism through time. Large sheet flows dominate the early stages of Inari activity (units *fl_{1a}* and *fl_{1b}*). These flows are uplifted and

dissected by circumferential and radial fractures; some fractures serve as outlets for later localized lava flows (unit *fl₂*). Continued deformation is recorded by interior stepping of circumferential normal faults associated with deflation of the corona’s internal support.

A large cluster of three moderately sized, corona-like (>50 km diameter) structures and two to five small (<30 km diameter) quasi-circular volcano-tectonic centers lie to the east of Tahmina Planitia, to the west of Gauri Mons, and to the south of Kuanja Chasma (lat 21.5° S., long 98° E.). Although some individual flows appear to emanate from within the individual centers, penetrative fabrics of closely spaced tectonic structures occlude much of the temporal relations within the center of the cluster. However, near the margin (for example, lat 21.5° S., long 97° E.), a portion of preexisting material (unit *fb₂*) is preserved in the less deformed region. Thus, in this locality where the base material can be recognized, the marginal deformation of the cluster is younger than unit *fb₂*. Unfortunately, this temporal relationship cannot be extrapolated to the remainder of the cluster because the origin of the base material is unknown. Therefore, the cluster is lumped into unit *fchu*, which contains multiple sites of isolated volcanic and tectonic activity having ambiguous temporal relations. The cluster is differentiated from the bulk of map unit *fchu* by a stipple pattern representing areas of penetrative secondary structures.

Coronae within V-35 (Inari and the cluster), as with many coronae on Venus, show a strong spatial correlation with chasma features (Hamilton and Stofan, 1996; Stofan and others, 2000). Structural trends from most coronae in V-35 merge with the Kuanja, Ralk-umgu, and Vir-ava Chasmata structures, commonly becoming indiscernible, and thus are lumped into unit *fchu*. This strong spatial correlation leads to speculation that coronae and chasmata result from the same internal processes with only surface morphologies differing due to crustal heterogeneities. V-35 map relations support current models that attribute coronae to Rayleigh-Taylor instabilities (Tackley and Stevenson, 1991) or mantle diapirs (Stofan and Head, 1990; Squyres and others, 1992; Stofan and others, 1992) originating above the apexes of cylindrical mantle convection cells (Hamilton and Stofan, 1996; Stofan and others, 1997). Coincident formation of coronae, spawned diapirs (thermal or compositional) from within broad mantle upwellings, and chasmata, intensely intruded linear zones serving as underground plumbing systems, may be responsible for significant mantle heat loss.

Wrinkle Ridges and Ridge Belts

Wrinkle ridges occur in the southwest corner of the map area (Tahmina Planitia). Multiple sets of generally north-trending ridges, which vary in amplitude and wavelength, support an alternative hypothesis that the units

in this region experienced a diachronous history of contraction with multiple episodes, rather than a punctuated period of wrinkle ridge development proposed by some workers (for example, Basilevsky and others, 1997). Units fb₂, fLS, and fTh each record some degree of east-west shortening, whereas unit fb₁ (which hosts east-northeast-trending large amplitude ridges) does not record such shortening; however, unit fb₁ does exhibit evidence of north-south extension, consistent with regional bulk strain (fig. 4, map sheet). Mechanical heterogeneities within the predominantly east-trending structural fabric of unit fb₁ could have resulted in a local strengthening of the crust and a resistance to deformation by the moderate wavelength north-trending ridges within unit fb₂. The change in structural orientation between the two structural suites (the unit fb₁ ridge belt and the north-trending wrinkle ridges) illustrates that the accommodation of contractional strain within the area has taken on a new orientation between events; however, this does not require a large variation in the orientation of the regional stress field.

Unit fb₂ is the oldest unit in the area that records wrinkle ridge deformation and displays two sets of ridges: one closely spaced (2–5 km) north-trending suite and a second moderately spaced (10–30 km) north-trending suite. Mechanical considerations would argue that the shorter wavelength suite reflects deformation of a thinner layer and that the longer wavelength suite reflects deformation of a thick layer. Thus, with continued shortening the layer might strengthen until it can no longer deform at the intrinsic wavelength and a new, more widely spaced wavelength would develop, or the two ridge suites could form synchronously, yet deform layers of different thickness like parasitic folds forming on a large fold train. Within Tahmina Planitia, the longer wavelength ridges tend to parallel and emphasize the presumably earlier formed ridges, which is also consistent with progressive deformation during the deepening of a lava flow cooling front.

Embayment relations between units fb₂, fLS, and fTh support a progressive evolution of short- to long-wavelength ridge suites. Unit fLS flows, as discussed previously, completely occlude the short-wavelength ridges and blanket the long-wavelength ridges of unit fb₂, whereas the distal portions of unit fTh flows clearly embay the topographic expression of the ridges that deform unit fb₂. In both cases, longer wavelength ridges also deform the younger units. Thus, the short-wavelength ridges predate the long-wavelength ridges, and the long-wavelength ridges formed diachronously relative to the emplacement of the volcanic flow units.

GEOLOGIC HISTORY

Without any absolute timing constraints (radiometric ages, isotope stratigraphy, biostratigraphy, or significant crater statistics; Hauck and others, 1998; Campbell, 1999),

true correlation (matching defined lithostratigraphic units by age) becomes highly suspect. Therefore, event stratigraphy or geologic history (Hansen, 2000) is the preferred method of displaying local sequences. Following Hansen (1991) a Sequence of Map Units (SOMU) chart is constructed in which the V–35 quadrangle is divided into three geographic regions where embayment and cross-cutting relationships robustly constrain relative timing: western, northeastern, and south-central to southeastern regions. The logic behind this methodology is that each region consists of a particular basal unit(s) that becomes the host for subsequent volcanic and tectonic activity. Without the means to relate the spatially disparate bases to one another, robust correlation is impossible. The SOMU also contains a section (widespread units) that includes map units that display either multiple temporal relations (unit fchu) or are made up of spatially disparate pieces that cannot be placed in any one particular region (units ti, c, and cf). In addition to the regional divisions, we provide information about the structural development and relative crater emplacement within each region.

The standard convention of placing older events at the bottom and younger events at the top applies; however, temporal relations between units are implied only within a vertical column of touching map units. Units that touch within the sequence chart are in contact on the map; this provides a means to depict the degree of certainty of relative time relationships. For example, in the western region, unit fLS is in contact with units tO, fb₁, and fb₂, and unit fLS is younger than these units. However, because unit tO, unit fb₁, and unit fb₂ are not in contact with each other, temporal relations are ambiguous. One further convention of the sequence chart is the height of the individual unit boxes; a box of equal height represents each unit, with the exception of unit fchu, unit c, and unit cf. Equal height does not represent equal time but rather equal ambiguity. Because different processes (tectonic or volcanic) vary in duration and because we lack any absolute temporal constraints, we cannot delineate time boundaries between events. Therefore, each region is an individual attempt to illustrate robust temporal relations based on reproducible mapping observations.

Western Region Summary

Tessera of Ovda Regio, Lo Shen Valles flows, and the basal flow material, member 2, dominate the western region of V–35 and provide much of the relative timing constraints in this area. Numerous, spatially less expansive units can only be placed as older or younger than the regionally dominant units. This region lacks robust temporal relations because many of the units are spatially isolated.

The tessera terrain within Ovda Regio is envisaged as forming as a result of plume impingement on a thin

lithosphere (Hansen and others, 1997, 1999; Hansen and Willis, 1998; Phillips and Hansen, 1994). Deformation and volcanism can both be related to this event and exhibit intertemporal relations across the region (flows embay small-scale structures and flows are crosscut by structures throughout the crustal plateau; for example, Banks and Hansen, 2000). Lo Shen Valles flows are thought to form in response to lithospheric extension and diapirism related to the development of the Ix-Chel and Kuanja Chasmata.

Northeastern Region Summary

The northeastern region contains four units (unit tT, unit fR, unit fTr, and unit tu). Thetis Regio is the local base that Rosmerta Corona flows and Turan Planum flows embay. The relative timing of Rosmerta and Turan cannot be determined because they do not share a common contact. Although this region could be part of a much larger daisy chain of map-wide, relative temporal relations, it may imply correlation of spatially disparate bases. For this reason we chose to separate this region in order to emphasize the ambiguity (especially of the base units) between different parts of the quadrangle.

South-Central to Southeastern Region Summary

Flows of Inari Corona dominate the southeastern region. The oldest far-reaching flows (units fl_{1a} and fl_{1b}) embay three spatially separate base units (units bB, fs_C, and ti). Because these units lack spatial, embayment, or structural relations, their temporal relations are unconstrained. Three other units (units fl₂, fch_a, and fch_b) show temporal relations with the early Inari flows in addition to the base material. Each unit lies above, and thus is younger than, units fl_{1a} and fl_{1b}. Although within the eastern portion of Turan Planum, unit fch_b superposes and is younger than unit fch_a, this relation should not be extrapolated for the entire unit fch_b. West of Turan Planum unit fch_b is not in contact with unit fch_a, unit fl_{1b}, or unit fl₂, and therefore temporal relations are unconstrained. Flows of Gauri Mons show only one relative temporal relation with the southeast region through Boszorkany Dorsa, which is embayed by unit fG from the west. Thus, Gauri Mons is younger than Boszorkany Dorsa; however, it may be older, younger, or the same age as the flows from Inari Corona.

The V-35 quadrangle records a rich history of tessera development, corona formation, and chasma evolution. The geologic history is constrained by observed contact relations and structural interactions, which resulted in the construction of robust geographically oriented event stratigraphies consistent with the 1:5,000,000 scale of mapping. Mapping at a larger scale with a higher degree of detail may lead to the discovery of new relationships that are inconsistent with this mapping; however, readers are

encouraged to analyze such areas with specific questions in mind.

REFERENCES CITED

- Addington, E.A., 2001, A stratigraphic study of small volcano clusters on Venus: Icarus, v. 149, p. 16–36.
- Arvidson, R.E., Brackett, R.A., Shepard, M.K., Izenberg, N.R., Fegley, B., and Plaut, J.J., 1994, Microwave surface properties of Ovda Regio and surroundings, Venus: Icarus, v. 112, p. 171–186.
- Banks, B.K., and Hansen, V.L., 2000, Relative timing of crustal plateau magmatism and tectonism at Tellus Regio, Venus: Journal of Geophysical Research, v. 105, p. 17,655–17,667.
- Barsukov, V.L., and 29 others, 1986, The geology and geomorphology of the Venus surface as revealed by the radar images obtained by Venera 15 and 16: Journal of Geophysical Research, v. 91, p. 378–398.
- Basilevsky, A.T., and Head, J.W., 1998, The geologic history of Venus—A stratigraphic view: Journal of Geophysical Research, v. 103, p. 8531–8544.
- Basilevsky, A.T., Head, J.W., Schaber, G.G., and Strom, R.G., 1997, The resurfacing history of Venus, *in* Bougher, S.W., Hunten, D.M., and Phillips, R.J., eds., Venus II—Geology, geophysics, atmosphere, and solar wind environment: Tucson, University of Arizona Press, p. 1047–1084.
- Basilevsky, A.T., Pronin, A.A., Ronca, L.B., Kryuchkov, V.P., Sukhanov, A.L., 1986, Styles of tectonic deformations on Venus—Analysis of Venera 15 and 16 data: Journal of Geophysical Research, v. 91, p. 399–411.
- Bindschadler, D.L., DeCharon, A., Beratan, K.K., Smrekar, S.E., and Head, J.W., 1992, Magellan observations of Alpha Regio—Implications for formation of complex ridged terrains on Venus: Journal of Geophysical Research, v. 97, p. 13,563–13,577.
- Brown, C.D., and Grimm, R.E., 1997, Tessera deformation and the contemporaneous thermal state of the plateau highlands, Venus: Earth and Planetary Science Letters, v. 147, p. 1–10.
- Campbell, B.A., 1999, Surface formation rates and impact crater densities on Venus: Journal of Geophysical Research, v. 104, p. 21,951–21,955.
- Campbell, B.A., Campbell, D.B., and DeVries, C.H., 1999, Surface processes in the Venus highlands—Results from analysis of Magellan and Arecibo data: Journal of Geophysical Research, v. 104, p. 1897–1916.
- Crumpler, L.S., Aubele, J.C., Senske, D.A., Keddie, S.T., Magee, K.P., and Head J.W., 1997, Volcanoes and centers of volcanism on Venus, *in* Bougher, S.W.,

- Hunten, D.M., and Phillips, R.J., eds., *Venus II—Geology, geophysics, atmosphere, and solar wind environment*: Tucson, University of Arizona Press, p. 697–756.
- Ford, J.P., Plaut, J.J., Weitz, C.M., Farr, T.G., Senske, D.A., Stofan, E.R., Michaels, Gregory, Parker, T.J., 1993, *Guide to Magellan image interpretation*: Jet Propulsion Laboratory Publication 93–24, 148 p.
- Ghent, R.R., and Hansen, V.L., 1999, Structural and kinematic analysis of eastern Ovda Regio, Venus—Implications for crustal plateau formation: *Icarus*, v. 139, p. 116–136.
- Gilmore, M.S., Ivanov, M.I., Head, J.W., and Basilevsky, A.T., 1997, Duration of tessera deformation on Venus: *Journal of Geophysical Research*, v. 102, p. 13,357–13,368.
- Hamilton, V.E., and Stofan, E.R., 1996, The geomorphology and evolution of Hecate Chasma, Venus: *Icarus*, v. 121, p. 171–194.
- Hansen, V.L., 2000, Geologic mapping of tectonic planets: *Earth and Planetary Science Letters*, v. 176, p. 527–542.
- 2003, In situ partial melts on Venus—Evidence for ancient water?, *in* *Lunar and Planetary Science XXXIV*, abstract #1152: Houston, Lunar and Planetary Institute [CD-ROM].
- Hansen, V.L., Banks, B.K., and Ghent, R.R., 1999, Tessera terrain and crustal plateaus, Venus: *Geology*, v. 27, p. 1071–1074.
- Hansen, V.L., and Bleamaster, L.F., 2002, Distributed point source volcanism—A mechanism for “regional plains” resurfacing, Venus, *in* *Lunar and Planetary Science XXXIII*, abstract #1061: Houston, Lunar and Planetary Institute [CD-ROM].
- Hansen, V.L., Phillips, R.J., Willis, J.J., and Ghent, R.R., 2000, Structures in tessera terrain, Venus—Issues and answers: *Journal of Geophysical Research*, v. 105, p. 4135–4152.
- Hansen, V.L., and Willis, J.J., 1996, Structural analysis of a sampling of tesserae—Implications for Venus geodynamics: *Icarus*, v. 123, p. 296–312.
- 1998, Ribbon terrain formation, southwestern Fortuna Tessera, Venus—Implications for lithosphere evolution: *Icarus*, v. 132, p. 332–343.
- Hansen, V.L., Willis, J.J., and Banerdt, W.B., 1997, Tectonic overview and synthesis, *in* Bougher, S.W., Hunten, D.M., and Phillips, R.J., eds., *Venus II—Geology, geophysics, atmosphere, and solar wind environment*: Tucson, University of Arizona Press, p. 797–844.
- Hansen, W.R. ed., 1991, *Suggestions to authors of the reports of the United States Geological Survey, Seventh Edition*: Washington, D.C., U.S. Government Printing Office, 289 p.
- Hauck, S.A., Phillips, R.J., and Price, M.H., 1998, Venus—Crater distribution and plains resurfacing models: *Journal of Geophysical Research*, v. 103, p. 13,635–13,642.
- Izenberg, N.R., Arvidson, R.E., and Phillips, R.J., 1994, Impact crater degradation on Venusian plains: *Geophysical Research Letters*, v. 21, p. 289–292.
- Kaula, W.M., 1990, Venus—A contrast in evolution to Earth: *Science*, v. 247, p. 1191–1196.
- Kirk, R.L., Soderblom, L.A., and Lee, E.M., 1992, Enhanced visualization for interpretation of Magellan radar data—Supplement to the Magellan special issue: *Journal of Geophysical Research*, v. 97, p. 16,371–16,380.
- Ladeira, F.L., and Price, N.J., 1981, Relations between fracture spacing and bed thickness: *Journal of Structural Geology*, v. 3, no. 2, p. 179–183.
- Phillips, R.J., and Hansen, V.L., 1994, Tectonic and magmatic evolution of Venus: *Annual Reviews of Earth and Planetary Science*, v. 22, p. 597–654.
- Plaut, J.J., 1993, Stereo imaging, *in* Ford, J.P., and others, *Guide to Magellan image interpretation*: Jet Propulsion Laboratory Publication 93–24, p. 33–43.
- Schenk, P., and Moore, H.J., 1992, An unusual thick lava flow in Ovda Regio, Venus, *in* *Lunar and Planetary Science XXIII* [abs.]: Houston, Lunar and Planetary Institute, p. 1217.
- Squyres, S.W., Janes, D.M., Baer, G., Bindschadler, D.L., Schubert, G., Sharpton, V.L., and Stofan, E.R., 1992, The morphology and evolution of coronae on Venus: *Journal of Geophysical Research*, v. 97, p. 13,611–13,634.
- Stewart, E.M., and Head, J.W., 2000, Evidence for temporal continuity of deformation in the Baltis Vallis region of Venus from observations of canali topography, *in* *Lunar and Planetary Science XXXI*, abstract #1692: Houston, Lunar and Planetary Institute [CD-ROM].
- Stofan, E.R., Hamilton, V.E., Janes, D.M., and Smrekar, S.E., 1997, Coronae on Venus—Morphology and origin, *in* Bougher, S.W., Hunten, D.M., and Phillips, R.J., eds., *Venus II—Geology, geophysics, atmosphere, and solar wind environment*: Tucson, University of Arizona Press, p. 931–965.
- Stofan, E.R., and Head, J.W., 1990, Coronae of Mnemosyne Regio, Venus—Morphology and origin: *Icarus*, v. 83, p. 216–243.
- Stofan, E.R., Sharpton, V.L., Schubert, G., Baer, G., Bindschadler, D.L., Janes, D.M., and Squyres, S.W., 1992, Global distribution and characteristics of coronae and related features on Venus—Implications for origin and relation to mantle processes: *Journal of Geophysical Research*, v. 97, p. 13,347–13,378.
- Stofan, E.R., Smrekar, S.E., and Martin, P., 2000, Coro-

nae of Parga Chasma, Venus—Implications for chasma and coronae evolution, *in* Lunar and Planetary Science XXXI, abstract #1578: Houston, Lunar and Planetary Institute [CD-ROM].

Tackley, P.J., and Stevenson, D.J., 1991, The production of small Venusian coronae by Rayleigh-Taylor instabilities in the uppermost mantle: Eos, Transactions of the American Geophysical Union, v. 72, p. 287.

Walker, G.P.L., 1992, “Coherent intrusion complexes” in large basaltic volcanoes—A new structural model: Journal of Volcanology and Geothermal Research, v. 50, p. 41–54.

Wilhelms, D.E., 1990, Geologic mapping, *in* Greeley, Ronald, and Baston, R.M., eds., Planetary mapping: New York, Cambridge University Press, p. 208–260.

Table 1. Crater data for the Ovda Regio quadrangle (V-35).

Name	Lat (° S.)	Long (° E.)	Diameter (km)	Unit location	Ejecta blanket	Impact halo	Central peak	Rim	Interior flooding	Deformation and notes
Bonnin	6.2	117.6	28.5	tT, fR	Y	N	?	Y	Y	No deformation; partial modification of interior by shield volcanism and mass wasting
Chloe	7.3	98.6	18.6	tO	Y	N	Y	Y	Y	No deformation; source of moderately dark, floor material is unknown
de Beausoleil	5.0	102.8	27.8	tO	Y	N	Y	Y	N	No deformation; ejecta blankets pre-existing structures
Denise	14.4	94.2	~2	fchu	Y	N	N	Y	N	No deformation
Elma	10.1	91.1	10.2	fLS	Y	N	Y	Y	N	Deformed by concentric fractures associated with nearby caldera collapse
Fukiko	23.1	105.7	13.9	fG	Y	N	N	Y	Y	No deformation; fluidized ejecta up to 75 km, interior modification by shield volcanism
Gail	16.1	97.5	~10	fchu	Y	N	N	Y	N	Cut by northwest-trending fractures
Helga	10.4	116.7	8.8	tT	Y	N	N	Y	N	No deformation
Jennifer	4.6	99.8	9.6	tO	Y	N	N	Y	N	Very low strain recorded in the form of tilting associated with broad wavelength, crustal plateau, marginal folds
Jhirad	16.8	105.6	50.2	fl _{1a} , bB	Y	?	Y	Y	Y	East-west fractures may pre- or post-date crater ¹ ; fluidized ejecta follows pre-existing north-south ridge belt, flows exceed 300 km
Makola	3.8	106.7	16.6	tO	Y	N	N	Y	Y	Very low strain recorded in the form of tilting associated with broad wavelength, crustal plateau, marginal folds
Maltby	23.3	119.7	36.6	fl _{1b}	Y	N	Y ²	Y	Y	Dissected by radial fractures associated with Inari Corona
Salika	5.0	97.7	12.5	mma	Y	N	N	Y	N	No deformation; ejecta blankets pre-existing structures
Sullivan	1.4	110.9	32	fitb	Y	N	Y	Y	Y	No deformation; volcanic modification of ejecta and interior floor
Teura	12.3	90.1	9.3	fLS	Y	N	N	Y	Y	No deformation; ejecta, rim, and interior are modified by a sinuous channel
unnamed crater	7.8	97.9	~2	tO	N	N	N	Y	N	Elevated rim blanketed with mm _a material
Yonge	14.0	115.1	42.8	fchu	Y	N	Y	Y	N	East-west trending fractures partially dissect the ejecta blanket
Zosia	18.9	109.2	10.5	fl _{1a}	Y	N	Y	Y	N	No deformation
Zulma	7.7	102	11	tO	N	N	N	Y	N	No deformation

¹East-west fractures show evidence of facilitating the movement of fluidized ejecta away from the impact site. One interpretation is that these fractures existed prior to the impact event and simply served as open pathways for the transport of the fluidized ejecta. However, a second interpretation is that the fractures represent dikes that postdate the impact event. Dikes, propagating upwards, part the surface and then provide lava as an agent to remobilize unconsolidated ejecta material.

²Central peak partially destroyed.